

# Polyaniline/Clay Nanocomposites-Synthesis and Characterization

Madhab Upadhyaya

Department of Chemistry, Chaiduar College, Gohpur, Assam, India

## ABSTRACT

Nanocomposites of polyaniline (PANI) with Na<sup>+</sup>-montmorillonite clay (MMT) were synthesized by emulsion polymerization method. Dodecylsulphuric acid (DSA) served the dual purpose of dopant and emulsifier. Analysis of X-ray diffraction results demonstrated the intercalation of PANI-DSA between the clay layers at the nanoscale level. The interaction between the intercalated PANI-DSA and clay layers was observed from FTIR spectra. The results of thermo gravimetric analysis showed the improved thermal stability of the nanocomposite materials. The dc conductivity was observed in the range 0.033-3.214 Scm<sup>-1</sup> at room temperature which found to be dependent on the loading of clay and dopant concentration. The morphology of the composite was investigated by scanning electron microscope and the morphology changed with the variation of MMT loading.

**KEYWORDS:** Polyaniline, MMT, nanocomposite, emulsion, intercalation, DSA

## 1. INTRODUCTION

The class of  $\pi$ -conjugated polymers has attracted attention because of their potential application as new electrical materials dependent on their redox properties. Among the  $\pi$ -conjugated polymers polyaniline is a promising material for commercial applications because of its several user friendly properties such as high conductivity [1], unique redox properties [2], easier method of preparation [3], good chemical and environmental stability [4,5] and low cost. It has been used in the pristine form as well as blends and composites. The intercalation of an organic guest into an inorganic host to fabricate nanocomposite materials has generated considerable research interest as the resultant materials are likely to have high potential for advanced electronic, magnetic, optical and sensing applications [6]. Such nanocomposites are made up of multilayer sandwich like elements in which polymer chains are sandwiched between ultrathin sheets of inorganic materials [7]. Such confinement of polymer is expected to lead to a high degree of order in polymer structure and enhanced thermal and oxidative stability. Intercalation of polyaniline in layered inorganic host is an example of such inorganic-organic hybrid material. The formation of PANI

composites with inorganic materials gives rise to new synergistic properties which cannot be attained in the pristine polymer [8]. Among the inorganic layered host materials montmorillonite clay (MMT) is the one widely used in nanocomposites because of its small particle size, low cost, good chemical resistance and well known tendency for intercalation [9]. The lamella of MMT constructed from an octahedral alumina sheet sandwiched between two tetrahedral silica sheets exhibits a net negative charge on the surface layers due to substitution of some Al<sup>+3</sup> ions by Mg<sup>+2</sup> ions. Cations such as Na<sup>+</sup> and Ca<sup>+2</sup> are present between layers to compensate the net charge, The swelling of MMT in water results in an increase in interlayer spacing which enables the penetration of clay layers by relatively large sized molecules. Mehrotra *et.al.*[10] and Wu and coworkers [11] investigated the intercalative polymerization of aniline in fluorohectorite and sodium montmorillonite respectively. Narkis and others [12] studied the composites of polyaniline and organically modified montmorillonite. The work of Nasimento *et.al.*[13] dealt with the spectroscopic characterization of polyaniline-clay composites prepared by polymerization of aniline in an aqueous suspension of

**How to cite this paper:** Madhab Upadhyaya "Polyaniline/Clay Nanocomposites-Synthesis and Characterization"

Published in International Journal of Trend in Scientific Research and Development (ijtsrd), ISSN: 2456-6470, Volume-6 | Issue-4, June 2022, pp.357-368, URL: [www.ijtsrd.com/papers/ijtsrd49979.pdf](http://www.ijtsrd.com/papers/ijtsrd49979.pdf)



IJTSRD49979

Copyright © 2022 by author(s) and International Journal of Trend in Scientific Research and Development Journal. This is an Open Access article distributed under the terms of the Creative Commons Attribution License (CC BY 4.0) (<http://creativecommons.org/licenses/by/4.0>)



MMT and camphor sulphonic acid. Yang and Chen [14] modified MMT with quaternary ammonium salt to synthesise nanocomposites with polyaniline. Binitha *et.al.*[15] used H<sub>2</sub>O<sub>2</sub> instead of commonly used oxidant persulphate for polymerization of aniline in presence of montmorillonite. An intercalated composite of polyaniline and illite clay exhibiting dendritic structure was described by Sing *et. al.*[16]. Kim *et.al.* [17-19] pioneered the emulsion intercalation method to synthesise polyaniline-MMT nanocomposites. They used dodecyl benzene sulphonic acid (DBSA) as dopant and emulsifier. To the best of our knowledge there is no report of using dodecyl sulphuric acid (DSA) for the synthesis of PANI-MMT composite by emulsion-intercalation method. Herein we report the synthesis and characterization of PANI-MMT nanocomposites synthesized by emulsion-intercalation method in presence of dodecylsulphuric acid (DSA), playing the role of both emulsifier and dopant.

## 2. Experimental

### 1.1. Materials and methods

Aniline (Merck, India) was distilled under reduced pressure before use. Dodecylsulphuric acid (DSA) was synthesized from sodium dodecyl sulphate by a cation exchange reaction using Amberlite IR-120 resin. Ammonium persulphate (APS), acetone and methanol (Merck, India) were analytical grade chemicals and were used as received without further purification. Na<sup>+</sup>-Montmorillonite clay was procured from USA (Clay Mineral Society-USA) and was used after purification by sedimentation technique.

### 1.2. Synthesis

#### 1.2.1. Purification of montmorillonite

MMT contains coarser impurities like sand and silt. It was purified by sedimentation technique [20]. 10 g of Na<sup>+</sup>-MMT was added to 500 mL distilled water and stirred for 2 h to form a 2% aqueous suspension of the clay. The suspension was allowed to stand undisturbed for 12 h. The heavy blackish particles at the bottom were rejected and the upper part of the clay suspension was siphoned out to flat trays. The trays were allowed to dry in hot air oven at 50-60°C and the purified clay was hand ground in agate mortar and kept in dry bottles.

#### 1.2.2. Preparation of dodecyl sulphuric acid (DSA)

10 g sodium dodecyl sulphate (SDS) was added to 500 mL distilled water and stirred well for 1 h and kept undisturbed for 2 h to obtain a clear solution. A cation exchange column was prepared with Amberlite IR-120 resin. The resin was carefully washed with 0.1 M HCl before the preparation of the column. The SDS solution was passed through the column very slowly and when methyl orange indicator indicated the acidic nature of the eluent, it was collected in a flask. The eluent so obtained is the dodecyl sulphuric acid (DSA). Its strength was determined by titrating with standard Na<sub>2</sub>CO<sub>3</sub> solution using methyl orange indicator.

#### 1.2.3. Synthesis of nanocomposites of polyaniline and Na<sup>+</sup>-MMT

Nanocomposites of polyaniline and Na<sup>+</sup>-MMT (PANI/MMT nanocomposites) were prepared by emulsion polymerization technique. Two sets of experiments were done. In one set, the DSA contents were varied while in the other the MMT contents were varied.

#### 1.2.4. Synthesis of PANI/MMT nanocomposites with varying amounts DSA.

50 mL of water was added to 0.093 g (10% by weight of aniline) of MMT taken in a beaker and stirred well with a magnetic stirrer to prepare a suspension. It was then sonicated in ultrasonic bath for 20 minutes to swell the clay. DSA was mixed with aniline monomer at various molar ratios as detailed in table 1 and cooled to 0-5°C. The solution containing aniline and DSA was added into the clay suspension with stirring for 1 h and kept undisturbed for 48 h allowing aniline to diffuse into the clay layers. After 48 h, 0.456 g (0.01 mol) ammonium persulphate (APS) dissolved in 20 mL water and cooled to 0-5°C was added very slowly into the suspension with constant stirring. Soon the polymerization reaction started turning the colour of the reaction mixture from light green to deep green. Stirring was continued for 2 h and the reaction mixture was left undisturbed for another 6 h. The precipitate was separated under centrifugation at 10000 rpm and was washed several times with water and methanol to remove excess surfactant and oligomers. It was finally dried at 50°C and stored in desiccators.

**Table 1 Synthesis of PANI/MMT nanocomposites with varying concentration of surfactant (DSA).**

Sl. No.	Aniline (mol)	MMT (%)	DSA (mol)	APS (mol)	Molar ratio Aniline: DSA	Sample Code
1.	0.01	10	0.010	0.01	1:1	PANI-DSA/MMT-1
2.	0.01	10	0.015	0.01	1:1.5	PANI-DSA/MMT-2
3.	0.01	10	0.020	0.01	1:2	PANI-DSA/MMT-3
4.	0.01	10	0.025	0.01	1:2.5	PANI-DSA/MMT-4
5.	0.01	10	0.030	0.01	1:3	PANI-DSA/MMT-5
6.	0.01	0.00	0.020	0.01	1:2	PANI-DSA

### 1.2.5. Synthesis of PANI-MMT nanocomposites with varying content of MMT

50 mL of water was added separately to varying amounts of MMT as shown in table 2 and stirred well with a magnetic stirrer to prepare suspensions. Each suspension was then sonicated in ultrasonic bath for 20 minutes for swelling of the clay. 0.020 mol DSA was mixed with 0.931 g (0.01 mol) aniline monomer and cooled to 0-5°C.

**Table 2 Synthesis of PANI/MMT nanocomposites with varying MMT content.**

Sl. No.	Aniline (mol)	MMT (%)	DSA (mol)	APS (mol)	Aniline to DSA molar ratio	Sample Code
1.	0.01	10	0.020	0.01	1:2	PANI-DSA/MMT-3
2.	0.01	15	0.020	0.01	1:2	PANI-DSA/MMT-6
3.	0.01	25	0.020	0.01	1:2	PANI-DSA/MMT-7
4.	0.01	30	0.020	0.01	1:2	PANI-DSA/MMT-8

The solution containing aniline and DSA was added to the clay suspension with stirring for 1 h and kept undisturbed for 48h to facilitate aniline diffusion into the clay layers. After 48h, 0.456 g (0.01 mol) ammonium persulphate (APS) dissolved in 20 mL water and cooled to 0-5°C was added very slowly into the suspension with constant stirring. Soon the polymerization reaction started with the change in colour of the reaction mixture from light green to deep green. Stirring was continued for 2 h and the reaction mixture was kept undisturbed for another 6 h. The precipitate was separated under centrifugation at 10000 rpm and was washed several times with water and methanol to remove excess surfactant and oligomers. It was then dried at 50°C and stored in a desiccator.

### 1.3. Characterization and testing

The UV-Vis absorption spectra were recorded in the 300–900 nm range in a Shimadzu UV-1800 (Japan) spectrophotometer. FTIR spectra of all samples were recorded in a Shimadzu IR Affinity-1 (Japan) spectrophotometer as KBr pellet at room temperature in the range of 4,000–400 cm<sup>-1</sup>. Phase identification of finely powdered samples were performed with an X'Pert Pro X-ray diffractometer, Phillips with nickel-filtered Cu K $\alpha$  radiation (wavelength = 1.5414Å) in the 2 $\theta$  range of 5–40°. Thermogravimetric analysis (TGA) of the samples was carried out in a Perkin Elmer Pyris 1 TGA instrument at a heating rate of 10°C/min under N<sub>2</sub> atmosphere over a temperature range of 20–800°C. SEM micrographs were obtained in a JSM-6360 (JEOL) scanning electron microscope at an accelerating voltage of 20 kV. Electrical conductivities of the samples were measured at room temperature with dry-pressed pellets by standard four probe technique.

## 3. Results and discussion

### 1.4. X-ray diffraction (XRD) studies

Powdered X-ray diffraction (XRD) is an efficient analytical tool to study the extent of intercalation/ exfoliation in clay. Figure 1 shows the XRD patterns of MMT, PANI-DSA and PANI-DSA/MMT-3 nanocomposite. The XRD pattern of MMT showed peaks at 2 $\theta$  ~ 7°, 12°, 20°, 21°, 24°, 26° and 29°. The peak at 2 $\theta$  ~ 7° is due to (001) reflection and corresponds to the periodicity in the direction perpendicular to the clay axis (C-axis). In case of PANI-DSA, the peaks observed are at 2 $\theta$  ~ 20°, 25° and 26°. PANI-DSA is a semicrystalline material, which is indicated by the absence of low angle peak and presence of low intensity broad peaks at higher 2 $\theta$  values in its XRD spectrum. The characteristic band for PANI was observed at 2 $\theta$  ~ 25°. This is in consistence with literature [21, 22].

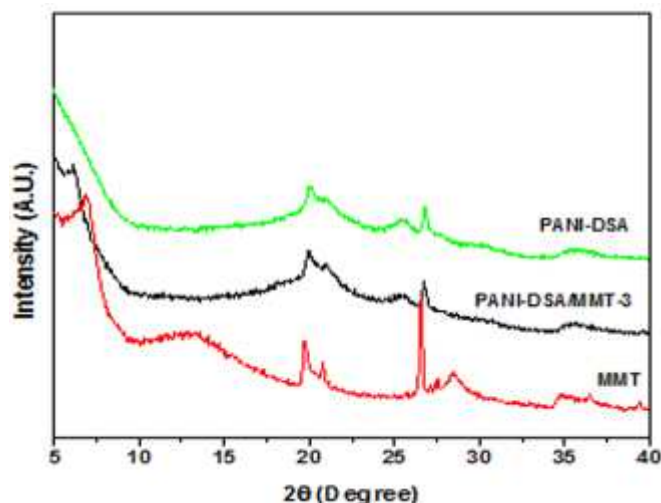


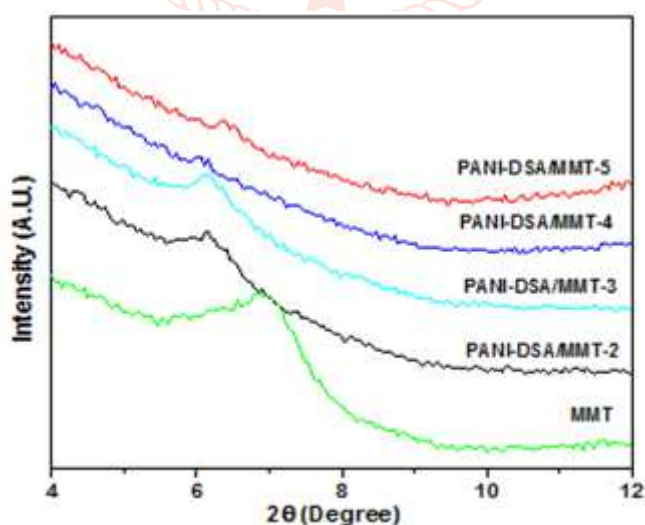
**Figure 1 XRD patterns of MMT, PANI-DSA and PANI-DSA/MMT-3**

The peaks observed in PANI-DSA/MMT nanocomposites are at  $2\theta \sim 6^\circ$ ,  $20^\circ$ ,  $21^\circ$ ,  $25^\circ$  and  $26^\circ$ . The XRD patterns of PANI-DSA and PANI-DSA/MMT are almost similar except for the peak at  $2\theta \sim 7^\circ$ . The pristine MMT peak observed at  $2\theta \sim 7^\circ$  which was absent in PANI-DSA is now shifted to  $2\theta \sim 6^\circ$  in PANI-DSA/MMT-3. This shift is due to the intercalation of the PANI-DSA between the clay layers. The d-spacing in the direction of c-axis of the clay sample estimated by using Bragg's equation [23]  $n\lambda = 2d\sin\theta$  was  $12.62 \text{ \AA}$  (table 3) in pristine MMT and was  $14.81 \text{ \AA}$  in PANI-DSA/MMT-3.

**Table 3 Increase in d- spacing as a result of intercalation of PANI in MMT**

Sample	$2\theta(^\circ)$	d-spacing ( $\text{\AA}$ )	Increase in d-spacing ( $\text{\AA}$ )
MMT	$\sim 7$	12.62	2.19
PANI-DSA/MMT-3	$\sim 6$	14.81	

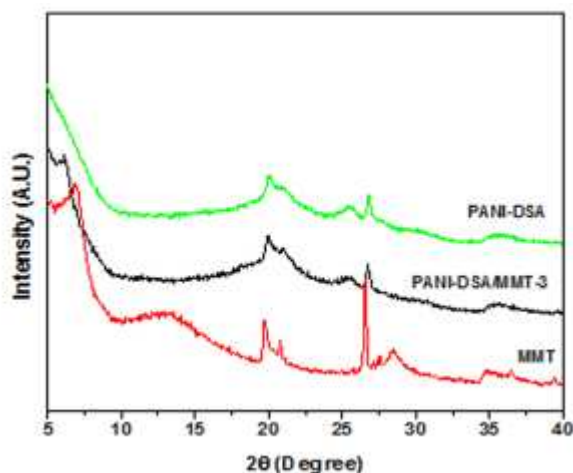
The increase in d-spacing ( $2.19 \text{ \AA}$ ) demonstrated the intercalation of PANI-DSA material inside the clay layers at the nanoscale level. During intercalation, the PANI-DSA chains get confined between the MMT layers and the distance between the MMT layers is increased depending on the dimension of the doped PANI chains, layer charge density and the functionality of the intercalating chains [24, 25]. Nascimento *et. al.*[26] polymerized aniline in MMT suspension using camphorsulphonic acid and reported XRD peaks at  $2\theta \sim 8^\circ$  and a halo at  $2\theta \sim 25^\circ$  which is very much similar to our observation in the present case. Cellik *et. al.*[27] observed a crystalline peak at  $2\theta \sim 9^\circ$  for MMT which was shifted towards lower angles in PANI-MMT nanocomposites due to the intercalation of PANI between MMT layers.



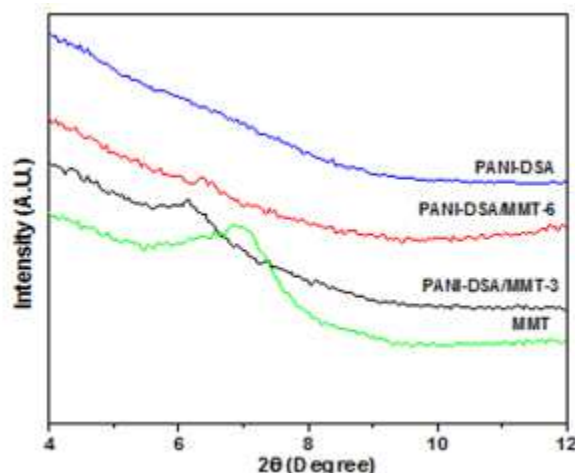
**Figure 2 XRD patterns of MMT, PANI-DSA and PANI-DSA/MMT with different molar concentrations of DSA**

Figure 2 shows the X-ray diffraction patterns of PANI/MMT nanocomposites with variations in the molar concentrations of DSA. In all cases the low angle peaks shifted to lower values in comparison to that of pristine MMT, indicating the intercalation of polyaniline chains between clay layers. But rise in the concentration of DSA decreases the extent of intercalation as is evident from the shifting of Bragg's diffraction peaks towards

higher values. Furthermore it was observed that the intensity of the low angle peak of the nanocomposite decreased with increasing molar concentration of DSA i.e increasing doping level. Similar observation was made by Kim *et. al.*[19] with dodecyl benzene sulphonic acid (DBSA) as the surfactant and doping agent. They believed that the formation of an aggregated bulkier form resulted in less effective intercalation. Brindley *et. al.* [28] also observed that the intercalation of alkyl chains having polar head group with clay surface forms self-assembled structure on the clay surface, rather than inside clay layers.



**Figure 3. XRD patterns of pure MMT, PANI-DSA and PANI-DSA/MMT nanocomposite with varying MMT contents**



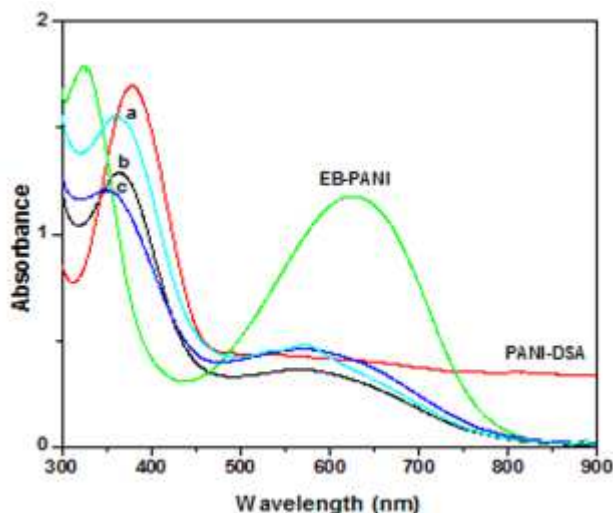
**Figure 4. Low angle XRD patterns of pure MMT, PANI-DSA and PANI-DSA/MMT nanocomposite with varying MMT contents**

Figure 3 and figure 4 show the X-ray diffraction patterns of PANI-DSA/MMT nanocomposites with varying MMT contents along with the X-ray diffraction patterns of pure MMT and PANI-DSA. Comparison of peak intensity of low angle peak for PANI-DSA/MMT-3 and PANI-DSA/MMT-6, it was evident that when the relative concentration of MMT doubled, the peak intensity decreased indicating disorganization in the layered structure leading to decrease in degree of crystallinity. The reason for this however is not clearly understood.

## 1.5. Spectral studies

### 1.5.1. UV-Vis spectral studies

UV-Vis spectroscopy is a sensitive tool for studying the nature of PANI-protonation. It provides evidence for the formation of polaronic structure on being doped by protic acids. The polaronic structure gives rise to conductivity in PANI. For the emeraldine base form of PANI (EB-PANI) generally two peaks are observed, one is due to  $\pi$ - $\pi^*$  transition for the benzenoid ring (324 to 370 nm) and the other due to benzenoid to quinoid transition (625 to 770 nm). On the otherhand for the emeraldine salt form of PANI generally three peaks may be obtained which are due to  $\pi$ - $\pi^*$  (312–380 nm), polaron- $\pi^*$  (370–440 nm) and  $\pi$ -polaron (768–782 nm) [29]. However the nature of the solvent influences the exact  $\lambda_{max}$  values. Figure 5 shows the UV-Vis spectra of EB-PANI, PANI-DSA and PANI-DSA/MMT nanocomposites. The EB-PANI has peaks at 324 nm and 625 nm corresponding to  $\pi$ - $\pi^*$  transition in the benzenoid ring and benzenoid to quinoid ring electronic transition respectively. In the PANI-DSA, both these peaks disappeared and instead a new peak appeared at 377 nm, which can be assigned to polaron- $\pi^*$  transition. The disappearance of benzenoid-quinoid transition peak is an indication of efficient doping process. Further, there are reports that if the energy gap between the  $\pi$ -band and polaron band disappear, only polaron- $\pi^*$  band is observed [30].



**Figure 5 UV-Vis spectra of EB-PANI, PANI-DSA, PANI-DSA/MMT-3 (a), PANI-DSA/MMT-4 (b) and PANI-DSA/MMT-6 (c)**

In the case of PANI-DSA/MMT nanocomposites two peaks were observed, one in the range of 360-400 nm and the other at around 600 nm. The peaks at 360-400 nm range could be assigned to polaron- $\pi^*$  transition. As similar peak was observed in PANI-DSA, it could be concluded that PANI-DSA chains are present in the structure of PANI-MMT nanocomposites. The presence of MMT marginally increase the energy difference between the polaron and  $\pi^*$  band resulting in a small blue shift of the absorption bands.

There is no peak at 600 nm in the UV-Vis spectrum of PANI-DSA, but it appears in all PANI-DSA/MMT nanocomposites indicating the presence of new chromophoric segments in the intercalated polyaniline structure. The appearance of bands at 620 nm and 670 nm was also observed by Nascimento *et al.*[13] during their investigation on aniline polymerization in MMT clay. They investigated the origin of these bands in detail by using standard compounds and concluded that these bands were due to the presence of azo bond and phenazine like segments in the confined polyaniline chains. Probably the peaks at  $\lambda \sim 600$  nm in PANI-DSA/MMT nanocomposites were also due to formation of such chromophoric segments as suggested by Nascimento *et al.*[13].

### 1.5.2. FTIR spectral studies

FTIR spectra of MMT, PANI-DSA, PANI-DSA/MMT-3, PANI-DSA/MMT-4 and PANI DSA/MMT-6 are shown in figure 6 and figure 7 which showed characteristic vibrations of both clay as well as the polymer. Peak assignments are shown in table 4. It is seen from the figure that  $\text{Na}^+$ -MMT has characteristic peaks at wavenumbers 3634, 1650, 1047, 793, 526 and 464  $\text{cm}^{-1}$ . The peak at 3634  $\text{cm}^{-1}$  arises from OH stretching vibration in  $\text{AlAlOH}$  and  $\text{AlMgOH}$  environments. The peak at 1650  $\text{cm}^{-1}$  is due to OH bending vibrations of adsorbed water [13]. The Si-O-Si stretching vibration peak which is very much prominent in MMT is seen at 1047  $\text{cm}^{-1}$ .

**Table 4 Prominent IR peaks in MMT, PANI-DSA and PANI-DSA/MMT nanocomposites and their assignments.**

MMT	PANI-DSA	PANI-DSA/MMT-3	PANI-DSA/MMT-4	PANI-DSA/MMT-6	Assignments
	3729	3737	3737	3737	N-H (secondary) stretching vibration
3634					OH stretching vibration in $\text{AlAlOH}$ and $\text{AlMgOH}$ environments
	3156				N-H stretching
	2942	2917	2931	2927	C-H stretching of quinoid ring
2341	2346	2346	2346	2346	$\text{CO}_2$ contamination
	1675	1672	1672	1672	C=C stretching mode of quinoid ring
1646	-	-	-	-	OH bending vibrations of adsorbed water.

	1533	1533	1533	1533	C=N stretching mode of benzenoid ring
	1411	1311	1292	1238	C-N and C-N <sup>+</sup> stretching mode of benzenoid ring
	1112	1051	1124	1045	C-H bending mode of quinoid ring
1047					Si-O-Si stretching.
793					O-H out-of-plane bending vibrations
	642	678	674	671	C-H out of plane bending of aromatic ring
526					Al-O stretching
461					Si-O bending mode

The peaks at  $793\text{ cm}^{-1}$  &  $526\text{ cm}^{-1}$  are due to OH out-of-plane and in-plane bending vibrations respectively. Peak at  $464\text{ cm}^{-1}$  may be assigned to Si-O bending mode [31]. In PANI-DSA the characteristic peaks for PANI are observed at wavenumbers  $3729$ ,  $3156$ ,  $2942$ ,  $1675$ ,  $1533$ ,  $1411$ ,  $1112$  and  $642\text{ cm}^{-1}$ . The peaks at  $3729\text{ cm}^{-1}$  and  $3156\text{ cm}^{-1}$  are due to N-H stretching and the one at  $2942\text{ cm}^{-1}$  is due to C-H stretching vibrations of quinoid ring. The two dominant peaks at positions  $1675$  and  $1533\text{ cm}^{-1}$  are assigned to C=C stretching mode of quinoid ring and C=N stretching mode of benzenoid rings respectively. The absorption band at  $1411\text{ cm}^{-1}$  corresponds to  $\pi$ -electron delocalization (C-N stretching). Almost equal intensity of the two peaks at  $1533$  and  $1411\text{ cm}^{-1}$  in PANI-DSA indicated that the synthesized PANI is in the emeraldine salt state [32]. Peak at  $1112\text{ cm}^{-1}$  is due to C-H bending mode of quinoid ring and the one at  $642\text{ cm}^{-1}$  corresponds to C-H out-of-plane deformation vibrations. These peak positions are very much similar with those found in literature [29, 33-34].

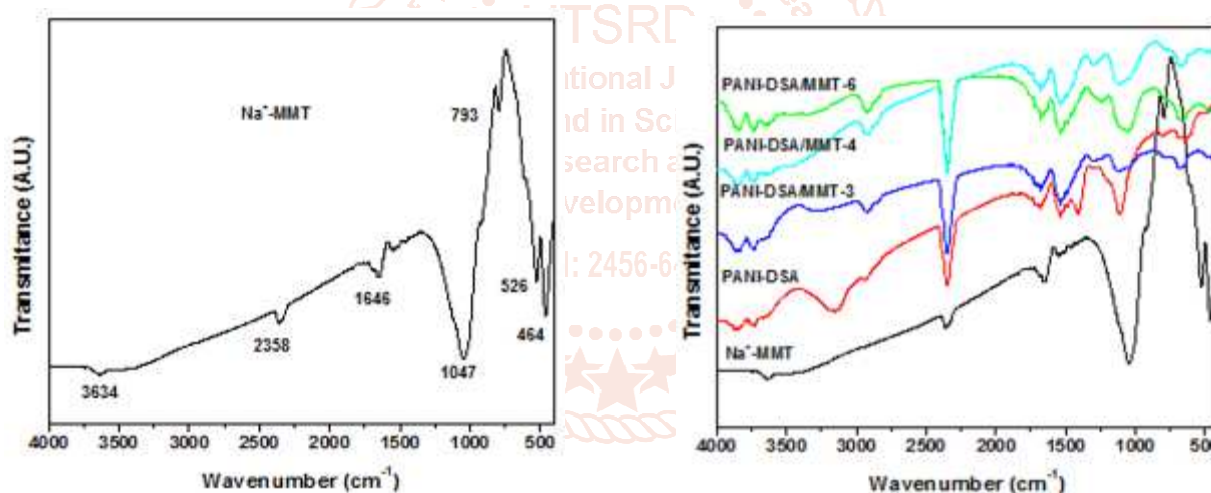


Figure 6. FTIR spectra of Na<sup>+</sup>-MMT

Figure 7. FTIR spectra of Na<sup>+</sup>-MMT, PANI-DSA and PANI-DSA/MMT nanocomposites

In PANI-DSA/MMT nanocomposites slight changes in peak positions and peak intensities are observed. The peak due to N-H (secondary) stretching appeared at  $3729\text{ cm}^{-1}$  in PANI-DSA, has been shifted to  $3737\text{ cm}^{-1}$  in all the PANI-DSA/MMT nanocomposites. This clearly indicates the presence of interaction between PANI-DSA and MMT. The peak due to C-H stretching vibration in quinoid ring appeared at  $2942\text{ cm}^{-1}$  in PANI-DSA was shifted to  $2917\text{ cm}^{-1}$  in PANI-DSA/MMT-3 and to  $2931\text{ cm}^{-1}$  in PANI-DSA/MMT-4 showing that this shift is dependent on DSA concentration. Larger amount of the dopant increases the degree of protonation which causes the peak position to change. A look at the peak positions of C-H stretching vibration in PANI-DSA, PANI-DSA/MMT-3, and PANI-DSA/MMT-6 shows that when the MMT content is higher, this shift is very small but its intensity increases as the MMT content increases. This is evident from table 2 and also from figure 6. Again, there is little change in the peak position due to the C=C stretching mode of quinoid ring which appeared at  $1675\text{ cm}^{-1}$  in PANI-DSA. It appeared at  $1672\text{ cm}^{-1}$  in all the nanocomposites namely PANI-DSA/MMT-3, PANI-DSA/MMT-4 and PANI-DSA/MMT-6. This peak is related to the degree of oxidation in the polymer. The same is the case with C=N stretching mode of benzenoid ring which appeared at  $1533\text{ cm}^{-1}$  in PANI-DSA and does not change its position in the nanocomposites. Thus the presence of MMT had no influence on these two stretching vibrations which are characteristics of PANI-DSA. Another important change observed in FTIR

spectra of PANI-DSA is the shifting of the peak at  $1411\text{ cm}^{-1}$  to lower values after the formation of nanocomposites with MMT. This peak corresponds to C-N and C-N<sup>+</sup> stretching mode of benzenoid ring. In PANI-DSA/MMT-3 this shift is from  $1411$  to  $1311\text{ cm}^{-1}$  and in PANI-DSA/MMT-4 it is from  $1411$  to  $1292\text{ cm}^{-1}$ . It is thus evident that the concentration of dopant (DSA) influences the amount of shift in absorption peak. In the nanocomposite PANI-DSA/MMT-6 having high content of MMT the shifting was found to be larger ( $1411 \rightarrow 1238\text{ cm}^{-1}$ ) compared to PANI-DSA/MMT-3 where the MMT content is lower. Although layered structure of the clay is supposed to hamper the protonation this high shifting may be due to structural changes in the PANI chains. Bober *et al.*[35] also observed similar shift of the peaks of PANI after nanocomposite formation with MMT and they accounted it to the overlapping with the spectra of MMT. Another important change observed in the FTIR spectra of PANI-DSA after nanocomposite formation with MMT is in the peak at  $1112\text{ cm}^{-1}$  (C-H bending mode of quinoid ring). This intense broad peak is associated with high electrical conductivity and a high degree of electron delocalization in PANI [37]. It is also observed that in case of PANI-DSA/MMT-3 this peak is shifted to  $1051\text{ cm}^{-1}$  while in PANI-DSA/MMT-4 with slightly higher DSA content it is shifted to  $1124\text{ cm}^{-1}$ . The Si-O-Si stretching frequency of MMT ( $1047\text{ cm}^{-1}$ ) is merged with the peak at  $1112\text{ cm}^{-1}$  (PANI-DSA) and appeared in the range  $1045$ - $1124\text{ cm}^{-1}$  in the nanocomposites. This is an indication of the strong interaction between MMT and PANI in the nanocomposites. Similar overlapping/merging of MMT peaks are also reported in literature [34, 37].

Again in case of PANI-DSA/MMT-6 with higher MMT content in comparison to PANI-DSA/MMT-3 the peak shifts to  $1045\text{ cm}^{-1}$  and this value is very much near to Si-O-Si stretching vibration peak of MMT itself. Kim *et al.*[19] suggests that the frequency shift to lower wave numbers of IR peaks ( $1411 \rightarrow 1238 - 1311\text{ cm}^{-1}$ ,  $1112 \rightarrow 1045$ - $1124\text{ cm}^{-1}$ ) of the PANI-DSA/MMT sample compared to PANI-DSA is due to the Coulomb interaction between the positive nitrogen of the intercalated PANI-DSA layer and the partially negatively charged surface of the clay. Such a frequency shift could also be accounted to the hydrogen bonded interactions between PANI and the basal surface of MMT (NH...O hydrogen bond). Similar results were reported by Reena *et al.*[38] while studying the role of amphiphilic dopants on the properties of PANI-Bentonite clay components. In the PANI-DSA/MMT nanocomposites, peaks at  $671$ - $678\text{ cm}^{-1}$  are due to C-H out-of-plane bending vibrations of 1, 2-disubstituted benzene ring [36]. In the case of PANI-DSA this vibration is characterized by a peak at  $642\text{ cm}^{-1}$ . After the formation of nanocomposites with MMT it was shifted to higher values. With the increase in DSA content there was a slight shift of the values to lower wavenumber as is evident from the values for PANI-DSA/MMT-3 ( $678\text{ cm}^{-1}$ ) and PANI-DSA/MMT-4 ( $674\text{ cm}^{-1}$ ). This shifting is related to the increase in the extent of protonation of PANI chains with increased concentration of DSA. With the rise in MMT content C-H out-of-plane bending vibration was further shifted as observed in PANI-DSA/MMT-6 ( $671\text{ cm}^{-1}$ ).

### 1.6. TGA studies

TGA studies are principally used for studying the degradation behavior of materials which provides the threshold temperature for materials applications. This study also provides a means for comparing the thermal stabilities of two materials. Further, TGA studies could also be used as a diagnostic tool as no two materials will produce the identical thermograms. Figure 8 shows the thermograms of EB-PANI, PANI-DSA and PANI-DSA/MMT-3 nanocomposite.

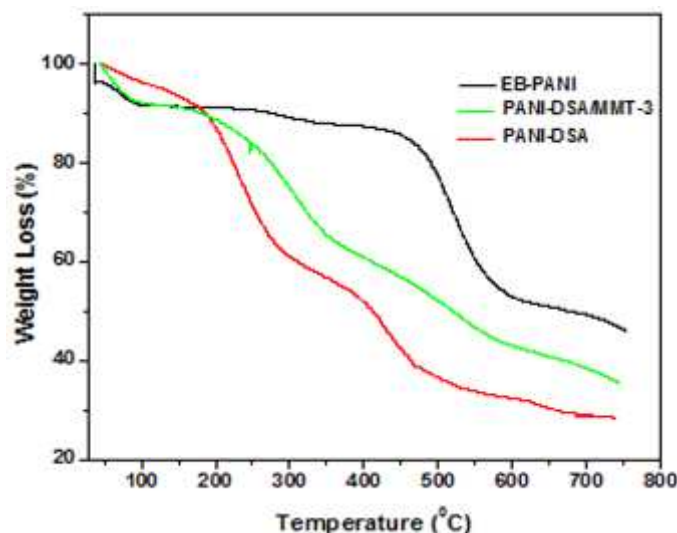


Figure 8 TGA plots of EB-PANI, PANI-DSA and PANI-DSA/MMT-3

As is evident from the thermograms the degradation pattern of PANI is influenced both by doping and the presence of clay. Doping always decreases the thermal stability. But smectite clays (MMT) are known to improve thermal stability of polymer-clay nanocomposites in comparison to pristine polymers [39].

**Table 5 Weight loss (%) and the corresponding temperature in °C of EB-PANI, PANI-DSA and PANI-DSA/MMT-3 nanocomposite**

Sample type	Weight loss (%)	Temperature (°C)
EB-PANI	10	100
	20	480
	30	520
	50	650
PANI-DSA	10	100
	20	220
	30	250
	50	410
PANI/DSA/MMT-3	10	100
	20	260
	30	320
	50	520

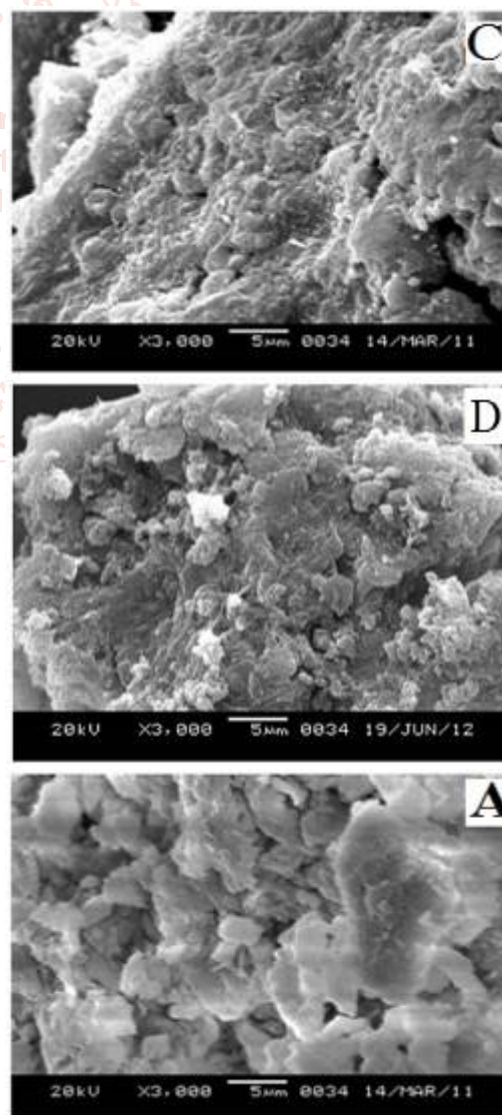
Table 5 shows the weight loss (%) and the corresponding temperature for EB-PANI, PANI-DSA and PANI-DSA/MMT-3. Comparing the values it is seen that the PANI-DSA/MMT-3 is thermally much more stable than PANI-DSA. The temperature for 50% weight loss in PANI-DSA is only 410°C while in PANI-DSA/MMT-3 it is 520°C. It is also observed that the temperatures for 20%, 30% weight losses are higher in PANI-DSA/MMT-3 than in PANI-DSA. The improvement of the thermal stability was due to clay sheets acting as thermal barrier.

In case of PANI, the thermogram shows three regions of weight loss, the first at around 100°C due to loss of moisture, the second in the region 200-300°C due to loss of dopant and the third in the range of 400-600°C due to scission of polymer backbone chains. Such three stage degradation is observed in case of PANI-DSA and PANI-DSA/MMT.

### 1.7. SEM studies

Scanning electron microscopic investigation provides information on the surface morphology of the polymeric material and is considered as an important tool to study the surface structure. The SEM images of pure Na<sup>+</sup>-MMT (image A), PANI DSA/MMT nanocomposites with varying MMT contents (images B to D) and with varying DSA contents (images D,F G) are shown in figure 9. SEM Image of PANI-DSA is shown in image E. PANI-DSA/MMT nanocomposites with varying amounts of DSA (images D, F and G). Pure Na<sup>+</sup>-MMT shows primary particles in the micrometer range that consists of face-to-face stacking crystallites (tactoids). These tightly bound tactoids are aligned to form ellipsoidal shaped agglomerations. The morphology of PANI-DSA

(image E) looks like clusters of agglomerated spherical particles. The size of cluster varies from 100 to 500 nm



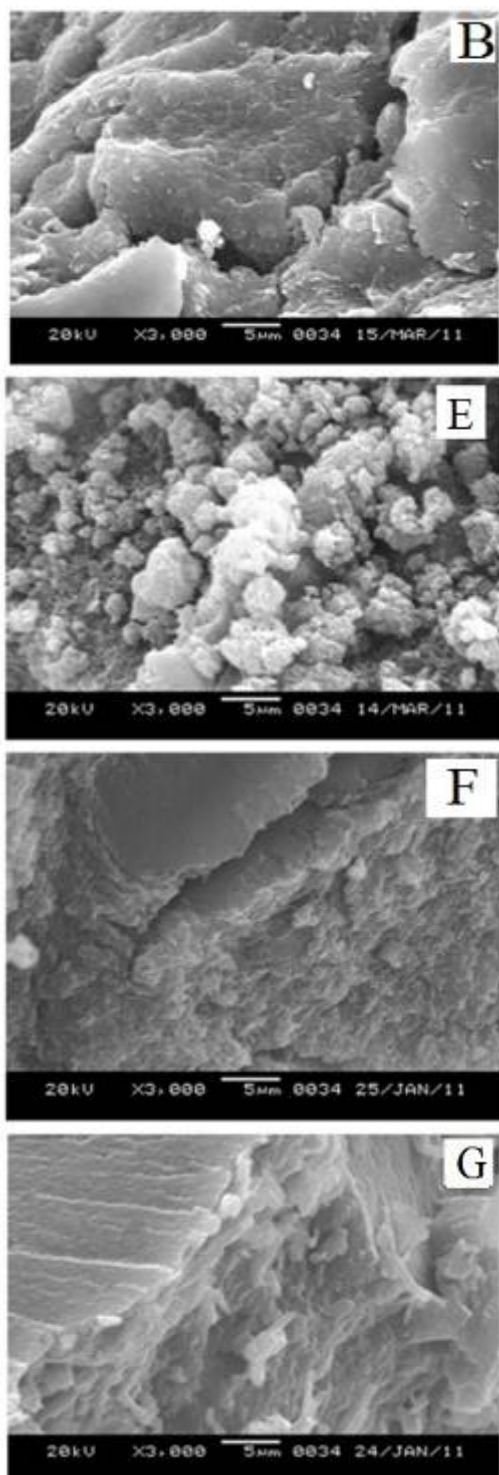


**Figure 9** SEM images of Na<sup>+</sup>-MMT (A), PANI-DSA/MMT-7 (B), PANI DSA/MMT-6 (C), PANI-DSA/MMT-3 (D) and PANI-DSA (E) SEM, PANI-DSA/MMT-2, (F) PANI-DSA/MMT-1(G)

The morphology of PANI-DSA/MMT nanocomposites with major MMT content (image B) is more or less similar to that of pure Na<sup>+</sup>-MMT (image A). As the MMT content decreases in the nanocomposites, the morphologies gradually changes from MMT type, where the tactoid plates dominate the image (image A), to morphologies where both tactoid plates and granular regions are seen (image D).

Morphologies are also dependent on the concentrations of dopant as is evident from images D, F and G where the composites vary only in the amount of dopant (DSA). As is evident, the self assembling process of PANI chains is dependent on the concentration of dopant as well as the intercalation process controlled by the clay. Probably several types of mutual interactions give rise to variety of assembling modes. According to Reena *et. al.*[38] these interactions may be non-covalent interactions among PANI chains and also different extent of ion-dipole interactions between clay and protonated PANI's

### 1.8. Conductivity studies

The conductivity of electroactive polymers depends on several factors like extent of doping, chain alignment, length of conjugation etc. In general the intercalation of electroactive polymers in clays or some other hosts produces materials with lower electrical conductivity than the pristine polymer free from the confinement effect [40, 41]. Some authors believe that clay hampers the connectivity between the particles containing intercalated conducting polymers, which lowered degree of electrical transport [11, 42].

For PANI-clay composites in particular, the rise in localization of charge carriers and decrease in the conjugation length of the organic chains was considered as the reason for lowering of electrical conductivity [30]. Nascimento *et. al.*[31] believed that appearance of chromophoric groups such as phenazine & azo in the PANI carbonic chains, which decreases the length of conjugation is also responsible for lowering of electrical conductivity in PANI-clay nanocomposites. MMT is non-conducting and its conductivity was found to be  $1.2 \times 10^{-9} \text{ Scm}^{-1}$ . Conductivities of PANI-DSA/MMT nanocomposites are of the order of  $10^{-1} \text{ Scm}^{-1}$  which is much higher than those reported earlier [29, 43-45]. The results of room temperature electrical conductivity of PANI-DSA and PANI-DSA/MMT nanocomposites are presented in table 6. The electrical conductivity of PANI-DSA/MMT nanocomposites decreased when MMT content is increased. The MMT content was varied from 10% to 30% by weight of aniline. The conductivity was lowest for PANI-DSA/MMT-8 with 30% MMT content in the composite. Similar conductivity behavior of PANI-MMT nanocomposites was reported by Nascimento *et. al.* [31] and Akbarinezhad *et. al.*[37]

Dopant (DSA) concentration also had an influence on the electrical conductivity of the nanocomposites. Increase in DSA amount resulted an increase in conductivity. Table 7 shows the electrical

conductivity values of the PANI-DSA/MMT nanocomposites having the same amount of MMT but with varying DSA contents. The DSA concentration was varied from 0.01 mol to 0.03 mol. It is evident from the table that increases in DSA (dopant) content results an increase in electrical conductivity. Kim *et. al.* [19] also reported similar effect on the electrical conductivity of PANI-MMT nanocomposites with the increase in the concentration of dopant dodecyl benzene sulphonic acid (DBSA).

#### 4. Conclusion

The nanocomposites of polyaniline and montmorillonite were synthesized successfully by emulsion polymerization process using dodecyl sulphuric acid (DSA) as the surfactant and dopant for the first time. The XRD results indicated the intercalation of PANI chains inside the clay layers. This results in a decrease in the conductivity with respect to pristine polymer. However, it was observed that at a particular loading of MMT, the conductivity increases with the rise in the dopant concentration. The observed conductivity values were at higher range than reported by others. The FTIR data showed the presence of varied type of interactions between the MMT and the confined PANI chains. The UV-Vis data indicated the possible formation of new chromophoric group as a result of polymerization in a confined environment. The composites are thermally stable than the pristine polymer. The morphology as reflected by SEM pictures is controlled by MMT content.

#### 5. Acknowledgements

The author is thankful to University Grants Commission (UGC-India) for awarding Teacher Fellowship under its Faculty Development Programme.

#### 6. References

- [1] Kingsborough RP, Swager TM (1998) *Adv Mater* 10:1100-1104.
- [2] Focke WW, Wnek GE, Wei YJ (1987) *J Phys Chem* 91:5813-5818.
- [3] Cao Y, Andrealta A, Heeger AJ, Smith P (1989) *Polymers* 30: 2305-2311.
- [4] Kohlman RS, Joo J, Epstein AJ (1996) In: Mark JA Edition physical properties of polymers Handbook, American Institute of Physics, Wiley, New work.
- [5] Trivedi DC (1997) In: Handbook of organic conductive molecules and polymers, Nalwa HS Edition J. Wiley & Sons, New York.
- [6] Porter TL, Hangerman ME, Eastman MP (1997) *Recent Research Dev Poly Sci* 1:1-17.
- [7] Kelah AA, Moet A (1994) *J Appl Polym Sci* 55:153-160.
- [8] Riede A, Helmstedt J, Riede V, Zemek J, Stejkal J (2000) *Langmuir* 16: 6240-6244
- [9] Kim JW, Kim SG, Hoi JH, Jhan MS (1999) *Macromol Rapid Commun* 20(8): 450-452
- [10] Mehrotra V, Giannelis EP (1991) *Solid State Commun* 77: 155-158.
- [11] Wu Q, Xue Z, Qi Z, Wang F(2000) *Polymer* 41: 2029-2032.
- [12] Jia W, Segal E, Kornemandel D, Lemhot Y, Narkis M, Siegmann A (2002) *Synth Met* 128: 115-120
- [13] Do Nascimento GM, Constantine VRL, Landers R, Temperini MLA (2004) *Macromolecules* 37: 9373-9385.
- [14] Yang SM, Chen KH (2003) *Synth Met* 135-136: 51-52
- [15] Binitha N, Suraja V, Yaakob Z, Sugunan S (2011) *Sains Malaysiana* 40(3): 215-217
- [16] Srivastava N, Sing Y, Sing RA (2011) *Bull Mat Sci* 34(4): 635-638
- [17] Kim BH, Jung JH, Kim JW, Choi HJ, Joo J (2001) *Synth Met* 117:115-118
- [18] Kim BH, Jung JH, Kim JW, Hoi HJ, Joo J (2001) *Synth Met* 121: 1311-1312.
- [19] Kim BH, Jung JH, Hong SH, Joo J, Epstein AJ, Mizoguchi K, Kim JW. Choi HJ (2002) *Macromolecules* 35: 1419-1423.
- [20] Jia W, Segal E, Kornemandel D, Lamhot Y, Narkis M, Siegmann A (2002) *Synth Met* 128: 115-120.
- [21] Messersmith PB, Giannelis EP (1994) *Chem Mater* 6: 1719-1725.
- [22] Pouget JP, Jozefowicz ME, Epstein AJ, Tang X, MacDiarmid AG (1991) *Macromolecules* 24(3): 779-789.
- [23] Guinier A (1983) *X-ray Diffraction*. Freeman WH. San Francisco.
- [24] Xia Y, Wiesinger JM Macdiarmid AG, Epstein AJ (1995) *Chem Mater* 7: 443-445.
- [25] Chen SA, Hwang GW (1995) *J American Chem Soc* 117: 10055-
- [26] Do Nascimento GM, Constantino VRL, Landers R, Temperini MLA (2006) *Polymer* 47: 6131-6139.

- [27] Celik M, Onal M, J Polym Res 2007; 14: 313-317.
- [28] Brindley GW, Moll WF (1965) Am Mineral 50: 1355-1370.
- [29] Abbas IB, Srasra E (2010) Reactive and Functional Polym 70: 11-18.
- [30] Epstein AJ, Ginder JM, Zhuo F, Woo HS, Tanner DB, Ritcher AF, Angelopoulos M, Huang WS, MacDiarmid AG (1987) Synth Met 13: 63-70.
- [31] Garai A, Kulia BK, Nandi AK (2006) Macromolecules 39: 5410-5418.
- [32] Wang T, Tan YJ (2006) Corrosion Science 48: 2274-2290.
- [33] Kulhankova L, Tokarsky J, Peikertova P, Kutlakova KM, Ivanek L, Capkova P (2012) J Phys and Chem of Solids 73 1530-1533.
- [34] Narayanan BN, Koodathil R, Gangadharan T, Yaakob Z, Saidu FK, Chandralayam S (2010) Mat Sci and Eng B 168: 242-244.
- [35] Bober P, Stejskal J, Spirkova M, Trchova M, Varga M, Prokes J (2010) Synth Met 160: 2596-2604.
- [36] Tang Q, Sun X, Li Q, Wu J, Lin J, Huang M (2009) Materials Letters 63: 540-542.
- [37] Akbarinezhad E, Ebrahimi M, Sharif F (2010) J Supercritical Fluids 59: 124-130.
- [38] Reena VL, Sudha JD, Pavithran C (2009) J Appl Polym Sci 113: 4066-4076.
- [39] Tjong SC, Meng YZ, Hay AS (2002) Chem Mater 14: 44-51.
- [40] Ruiz HE, Aranda P, Serratos JM (2004) In: Marcel Dekker. Eds.; Handbook of Layered Materials, Wiley, New York.
- [41] Chang TC, Ho SY, Chao KJ (1992) J Chin Chem Soc 39:209-212.
- [42] Kim BH, Hons SH, Joo J, Park IW, Epstein A J, Kim JW, Choi HJ (2004) J Appl Phys 95: 2697-2701.
- [43] Ballav N, Biswas M (2004) Polym Journal 36: 162-166.
- [44] Yoshimoto S, Ohashi F, Kameyama T (2005) J Polym Sci B: Polym Phys 43: 2705-2714.
- [45] Feng XM, Yang G, Liu Y, Hou WH, Zhu JJ (2006) J Appl Polym Sci 101: 2088-2094.

